 DOI: 10.1002/maco.201307492

Effect of heat treatment on the microstructure and corrosion behaviour of Mg–Zn alloys

H. R. Bakhsheshi-Rad*, E. Hamzah, M. Medraj, M. H. Idris, A. F. Lotfabadi, M. Daroonparvar and M. A. M. Yajid

Microstructure and corrosion behaviour in simulated body fluid of as-cast and heat treated Mg–*x*Zn ($x = 3$ and 6) alloys for different heat treatment times were studied. The results revealed that as-cast Mg–3Zn alloys consist of $Mg_{12}Zn_{13}$ phase and α-Mg matrix, while Mg–6Zn is composed of $Mg_{51}Zn_{20}$, $Mg_{12}Zn_{13}$ compounds and α-Mg matrix. After heat treatment of Mg–6Zn alloy at 340 °C, the $Mg_{51}Zn_{20}$ phase decomposed to the matrix and $Mg_{12}Zn_{13}$ while, the microstructure of Mg–3Zn remained unchanged. The results also indicated that heat treatment at 340 °C has little influence on the corrosion behaviour of Mg–3Zn. In contrast, heat treatment improved the corrosion resistance of the Mg–6Zn alloy as the decomposition of the $Mg_{51}Zn_{20}$ phase decreased micro-galvanic corrosion. The corrosion resistance of both as-cast Mg–3Zn and Mg–6Zn alloys marginally improved with increasing heat treatment times.

1 Introduction

Magnesium alloys are receiving high attention in the automotive industry because of their high strength to weight ratio in addition to other advantages [1–3]. Several researches also were carried out on the feasibility of using magnesium and its alloys as a new class of biodegradable materials for orthopaedic applications [4,5]. Magnesium plays a critical role in the human body and it is also the most principal constituent in human serum [6]. Zinc (Zn) is a crucial element for the human body and it is necessary for many biological functions. From materials viewpoint, Zn is known to increase age hardening response as it produces intermetallic compounds and refine the grain size [7]. Since zinc is more anodic to Fe and Ni that might be present as impurities in Mg alloys, it helps to overcome their harmful corrosion effect [8]. Hence, Zn-containing Mg alloys received great attention as most suitable candidate for biomedical applications. However, high corrosion rate and evolution of hydrogen gas of Mg alloys when exposed to human body fluids were major hurdles to their widespread application in various biodegradable applications [9–11]. Therefore alloying and heat treatment were applied for enhancement of Mg characteristics for implant use. Among magnesium alloys, Mg–Zn alloys exhibit a significant hardening effect and good mechanical properties [9]. *Zhou* et al. [12] showed that corrosion behaviour of AZ91D alloy was significantly affected by heat treatment. However, *Yang* et al. [4] indicated that corrosion behaviour of binary Mg–Dy alloys were less significantly affected by heat treatment. *Zhang* et al. [13] also suggested that the corrosion rate of Mg–15Y alloy considerably increased after heat treatment. Studies on the effect of heat treatment on the corrosion resistance of AZ91D, Mg–Y and Mg–Dy alloys had been widely reported [4,12,13]. However there is hardly any study on the microstructures and degradation behaviour of Mg–Zn alloys under various solid solution treatments. From a practical point of view, it is important to know the influence of heat treatment on the bio-corrosion behaviour of Mg–Zn alloy. Hence the present study focuses mainly on the microstructure and bio-corrosion behaviour of Mg–Zn alloys before and after T4 heat treatment.

2 Materials and methods

Magnesium alloys were prepared by melting 99.99% pure magnesium ingots and 99.99% pure zinc chips. The materials were melted by electrical resistance furnace under a protective atmosphere in a stainless steel crucible at 750 °C. The molten metal was maintained for around 45 min at the melting condition for stabilisation. After stabilising, molten metal with different Zn contents (3 and 6 wt%) was poured into mild steel moulds which had been preheated at 400 °C accompanied by a 30 s stirring process. Specimens 15 mm × 15 mm × 10 mm in size have been prepared from the as-cast alloys ingots, and the samples were then mechanically wet ground for microstructural observation.

H. R. Bakhsheshi-Rad, E. Hamzah, M. H. Idris, A. F. Lotfabadi, M. Daroonparvar, M. A. M. Yajid
Faculty of Mechanical Engineering, Department of Materials, Manufacturing and Industrial Engineering, Universiti Teknologi Malaysia, 81310 Johor Bahru, Johor, (Malaysia)
E-mail: rezabakhsheshi@gmail.com

M. Medraj
Department of Mechanical Engineering, Concordia University, 1455 De Maisonneuve Blvd. West, Montreal QC H3G 1M8, (Canada)

T4 solid solution heat treatment at 340 °C for 6, 12 and 18 h was carried out followed by hot water quenching at around 50 °C. For microstructure observation a scanning electron microscope (SEM) equipped with EDS analysis was used. Phase identification also was carried out by X-ray diffractometry (XRD). The immersion and electrochemical tests in simulated body fluid (SBF) were performed to investigate the corrosion behaviour of the magnesium alloys. The detailed preparation procedure of SBF and its ionic concentrations was proposed by *Kokubo* and *Takadama* [14]. The immersion test procedure was carried out based on the ASTM: G1-03.

3 Results and discussion

3.1 Microstructure analysis

The microstructure of as-cast and T4 treated Mg–3Zn alloy with various treatment times are summarized in Fig. 1. The as-cast Mg–3Zn microstructure consisted of primary α-Mg and secondary phases (Fig. 1a). However, after Mg–3Zn heat treatments at 6, 12 and 18 h the microstructure remained unchanged and an almost similar amount of secondary phases can be detected according to binary Mg–Zn alloy phase diagrams (Fig. 1b–d). Figure 1e shows that the as-cast Mg–6Zn microstructure consisted of primary α-Mg and secondary phases. However, the number of precipitates in T4 treated Mg–6Zn after 6 h significantly changed indicating that the decomposition of secondary phase into the matrix and $Mg_{12}Zn_{13}$ occurred (Fig. 1f). By increasing treatment time to 12 and 18 h, there is no significant change in the amount of secondary phases which can be because Mg dissolves Zn up to 8 wt% at the heat treatment temperature. Figure 2 shows SEM micrographs of as-cast Mg–3Zn, Mg–6Zn alloys and T4 heat treated alloys for 6 h. The Mg–3Zn microstructure consisted of α-Mg matrix and $Mg_{12}Zn_{13}$ secondary phases which resulted in the evolution of eutectic structure (α-Mg + $Mg_{12}Zn_{13}$) along the grain boundaries (Fig. 2a) indicating that the samples are not at equilibrium. The corresponding EDS analysis suggested that the dark area, which is composed of Mg and Zn, is related to $Mg_{12}Zn_{13}$. The microstructure of the T4 heat treated Mg–3Zn alloys shows no significant change (Fig. 2b). EDS analysis showed that the grain boundaries were enriched with Zn which indicated formation of $Mg_{12}Zn_{13}$ phase within the grain boundaries (Fig. 2b). However, Mg–6Zn alloy showed a higher amount of $Mg_{12}Zn_{13}$ compound in addition to $Mg_{51}Zn_{20}$ at grain boundaries compared to Mg–3Zn alloy (Fig. 2c). In this condition, $Mg_{51}Zn_{20}$ is formed due to the non-equilibrium solidification. EDS analysis further confirmed bright precipitates composed of Mg and Zn which are located along the grain boundaries (Fig. 2c). As molten metal is solidified, at first primary α-Mg formed and then rejection of alloying elements took place from the primary magnesium at liquid–solid interface as a result of more reduction in temperature. Consequently the Zn concentration, in the liquid remaining among magnesium dendrites, increases resulting in the formation of Zn-rich compounds. When the temperature of molten metal dropped to the eutectic reaction, intermetallic phase ($Mg_{12}Zn_{13}$) precipitated at the grain boundary. However in Mg–6Zn alloy, solidification is not achievable with the formation of $Mg_{12}Zn_{13}$ only. At the end of the solidification process, further decreasing the temperature caused the formation of $Mg_{51}Zn_{20}$ intermetallic phase. Heat treatment of Mg–3Zn alloy has a less significant effect on α-Mg. In this case a saturated solid solution of Zn in Mg forms and $Mg_{12}Zn_{13}$ precipitates out during cooling at much lower temperature. However, heat treatment of as-cast Mg–6Zn alloy resulted in decomposition of the $Mg_{51}Zn_{20}$ intermetallic compounds to reach to more formation of the α-Mg equilibrium phase (bright colour in Fig. 2d). The XRD pattern of the as-cast Mg–Zn alloys and T4 heat treated alloys (Fig. 3), indicates that only peaks corresponding to α-Mg matrix and $Mg_{12}Zn_{13}$ compound have been observed in the XRD pattern of Mg–3Zn alloy (Fig. 3a). Apart from the defined Mg and $Mg_{12}Zn_{13}$ reflections, the reflection of $Mg_{51}Zn_{20}$ appeared in Mg–6Zn alloy (Fig. 3b). However the intensity of $Mg_{12}Zn_{13}$

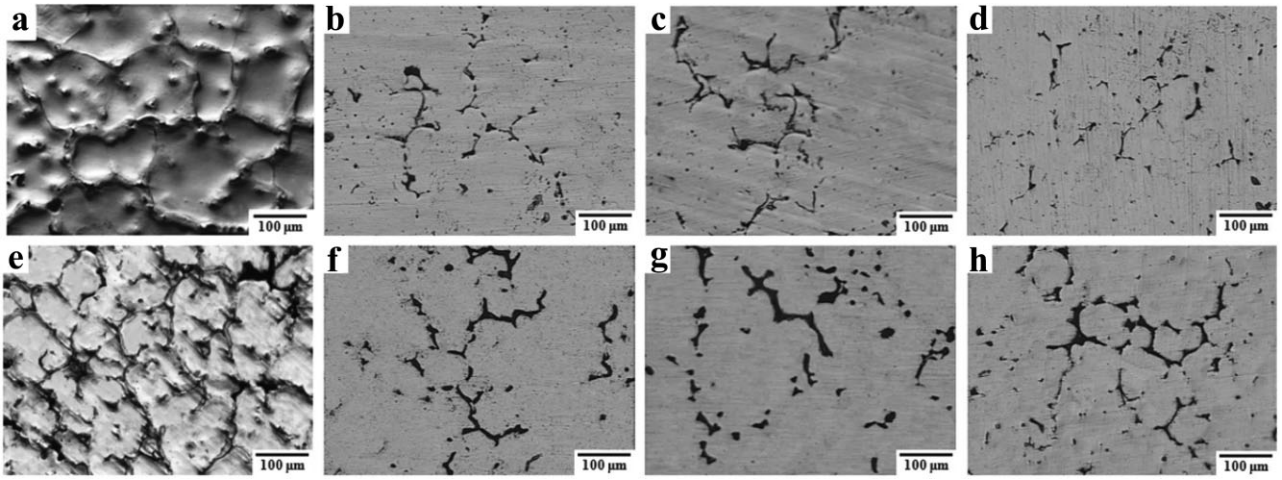

Figure 1. Optical microscopic images of (a) as-cast Mg–3Zn and heat treated alloys with different heat treatments time, (b) 6 h, (c) 12 h, (d) 18 h, (e) as-cast Mg–6Zn and heat treated alloys with different heat treatments time, (f) 6 h, (g) 12 h and (h) 18 h

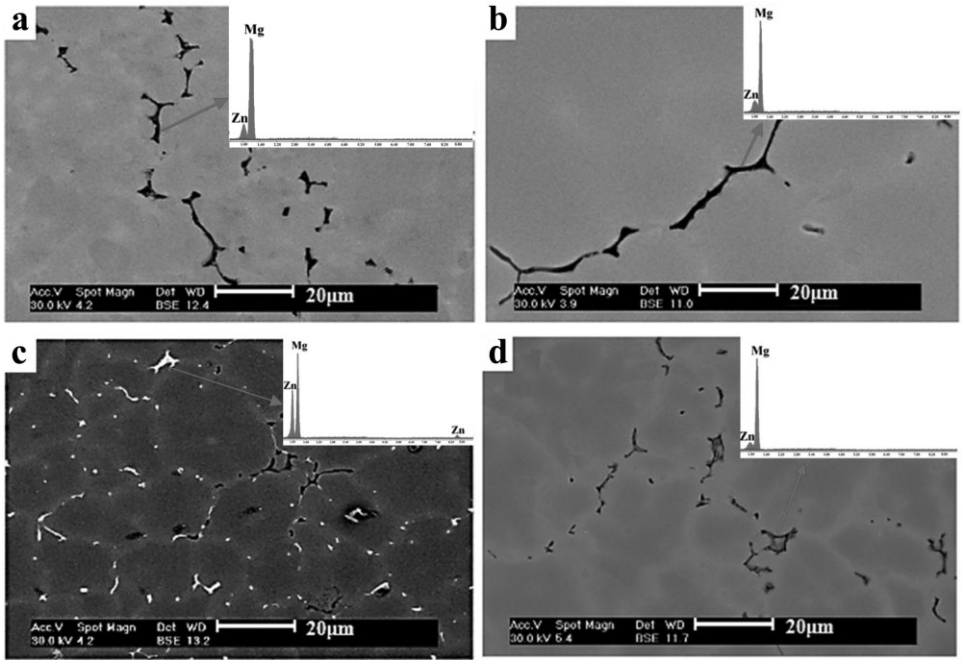

Figure 2. SEM micrographs with EDS results of as-cast and T4 heat treated alloys: (a) Mg–3Zn, (b) Mg–3Zn (6 h), (c) Mg–6Zn and (d) Mg–6Zn (6 h)

intermetallic phase in Mg–3Zn alloys marginally decreased with increasing heat treatment time to 18 h. The peaks related to the $Mg_{51}Zn_{20}$ phase were not detected after heat treatment, which indicates that the $Mg_{51}Zn_{20}$ phase decomposed completely to the Mg matrix and $Mg_{12}Zn_{13}$ phases. This result has good agreement with the binary Mg–Zn alloy phase diagrams (Fig. 4a and b). As can be seen when 3 wt% Zn is added, the alloy contains $Mg_{12}Zn_{13}$ compound. In this case, a 100 g of the overall material, at room temperature, is composed of 96.4 g Mg and 3.6 g $Mg_{12}Zn_{13}$ (Fig. 4c). Similar types of phases are observed in the T4 treated Mg–6Zn alloy but with different relative amounts where a 100 g of the overall material, at room temperature, is composed of 92.3 g Mg and 7.7 g $Mg_{12}Zn_{13}$ (Fig. 4d).

3.2 Electrochemical measurements

Figure 5 exhibited the polarisation curves recorded after 1 h exposure to Kokubo solution for as-cast Mg–3Zn, Mg–6Zn alloys and T4 heat treated alloys. As can be seen, Mg–6Zn alloy compared to Mg–3Zn alloy shows more negative corrosion potential, indicating that the corrosion behaviour of the alloy is significantly affected by the secondary phases. Mg–3Zn alloy presented lower corrosion potential ($-1731.7\,mV_{SCE}$) compared to the Mg–6Zn alloy ($-1759.2\,mV_{SCE}$). This is attributed to the increasing Zn content which leads to increasing amounts of the precipitation phases in the grain boundaries. The precipitate phases resulted in acceleration of the corrosion rate of the Mg–6Zn alloy because of the occurrence of higher galvanic corrosion between primary magnesium (α-Mg) and secondary phases [9,15]. The secondary phases act as a micro-cathode and play an essential function in increasing the corrosion rate of the Mg–6Zn alloy [4]. Mg–3Zn alloy heat treated for different times has a less significant influence on corrosion potential of the alloy. It was obvious from the polarisation curves, that all T4 heat treated Mg–3Zn alloys have similar corrosion potential (E_{corr}, V_{SCE}) to the as-cast Mg–3Zn alloy as the amount of the secondary phases after treatment

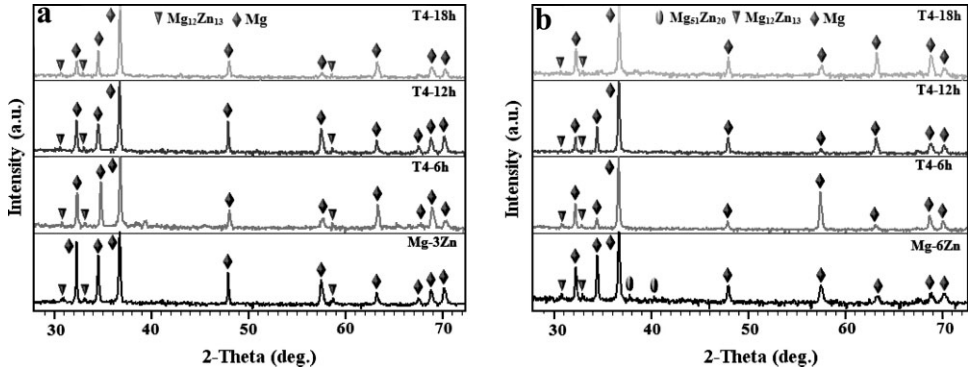

Figure 3. X-ray diffraction patterns of (a) Mg–3Zn and (b) Mg–6Zn alloys with different heat treatments time

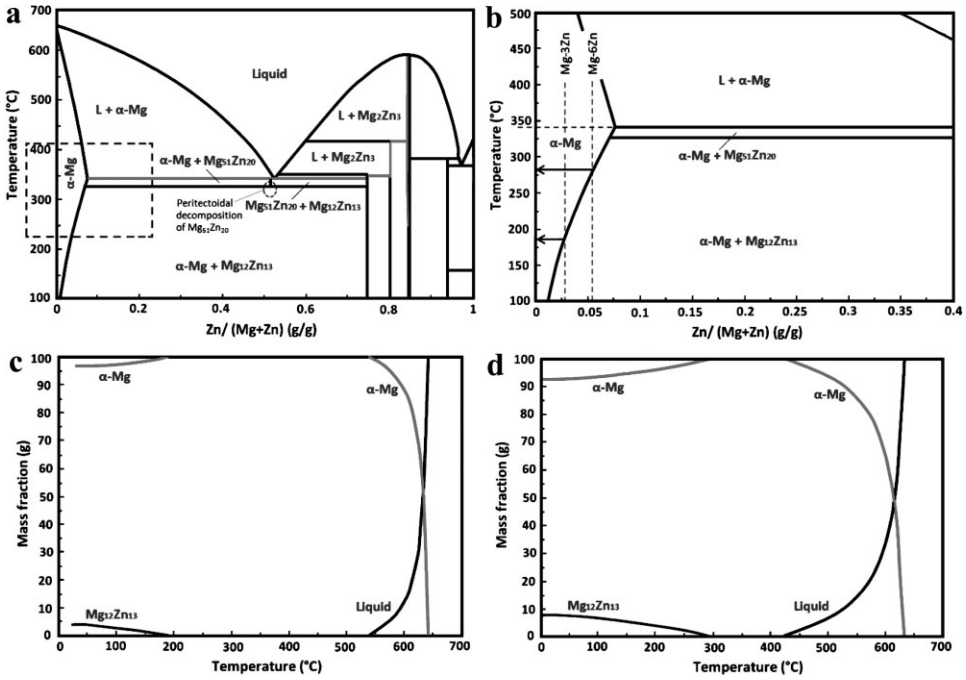

Figure 4. (a,b) Calculated phase fraction *versus* temperature for Mg–Zn and phase assemblage diagram of (c) Mg–3Zn and (d) Mg–6Zn

remains unchanged. The as-cast Mg–3Zn alloy corrosion current density (i_{corr}) was 228.3 μA/cm^2, slightly higher than the treated alloy for 6 h (223.6 μA/cm^2) and treated alloy for 12 h (216.2 μA/cm^2). Alloy heat treated for 18 h also indicated similar values to other treated alloys. It can be suggested that in the as-cast Mg–3Zn alloy, there is a galvanic couple where, the α-Mg phase plays the anode and the $Mg_{12}Zn_{13}$ phase performs the cathode role. The largest amount of the $Mg_{12}Zn_{13}$ secondary phase as cathode exhibits the highest hydrogen evolution rate [9]. As-cast Mg–6Zn alloy has a corrosion potential of −1759.2 mV_{SCE} and a corrosion current density of 270.8 μA/cm^2. However, heat treatment of Mg–6Zn alloy for 6 h shifted the corrosion potential upward (−1702.4 mV_{SCE}) and decreased the corrosion current density to 205.2 μA/cm^2. Generally, cathodic polarisation curves were assumed to indicate hydrogen evolution via water reduction; however, the dissolution of Mg was presented by anodic polarisation curves [16]. The reaction kinetics of cathode in as-cast Mg–6Zn alloys are faster comparing with heat treated Mg–6Zn alloy for 6 h, indicating the cathodic reaction, based on kinetic aspect, was more difficult in the as-cast alloys in comparison with treated alloy. As heat treatment time increased to 12 and 18 h the corrosion potential shifted to −1692.7 and −1682.3 mV_{SCE}, and the corrosion current density decreased to 198.4 and 191.5 μA/cm^2, respectively. Electrochemical parameters of as-cast in comparison with heat treated specimens are presented in Table 1. The corrosion rate (P_i) of samples obtained from the corrosion current density was calculated according to the following equation [13].

$$P_i = 22.85\, i_{corr} \quad (1)$$

According to Equation (1), Mg–3Zn and heat treated alloys showed similar corrosion rate in the range of 4.81–5.21 mm/year. However, Mg–3Zn treated alloys showed a lower corrosion rate compared to as-cast Mg–6Zn alloy. Larger amount of the $Mg_{12}Zn_{13}$ secondary phase leads to acceleration in hydrogen

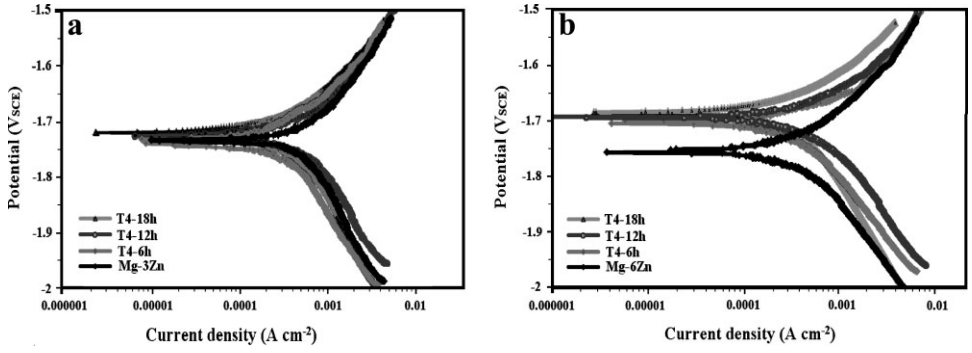

Figure 5. Polarisation curves of (a) Mg–3Zn and (b) Mg–6Zn alloys before and after heat treatment at different times and after immersion in Kokubo solution for 168 h

Table 1. Electrochemical parameters of as-cast and heat treated Mg–Zn alloy in Kokubo solution attained from the polarisation test

Alloy	Corrosion potential, E_{corr} (mV *vs.* SCE)	Current density, i_{corr} (μA/cm^2)	Cathodic slope, β_C (mV/decade) *versus* SCE	Anodic slope, β_a (mV/decade) *versus* SCE	Polarisation resistance, R_P (kΩ cm^2)	Corrosion rate, P_i (mm/year)
Mg–3Zn	−1731.7	228.3	312	126	1.70	5.21
T4 (6 h)	−1730.8	223.6	354	119	1.73	5.10
T4 (12 h)	−1724.6	216.2	387	115	1.78	4.94
T4 (18 h)	−1718.4	210.7	320	127	1.87	4.81
Mg–6Zn	−1759.2	270.8	344	117	1.40	6.18
T4 (6 h)	−1702.4	205.2	387	121	1.95	4.68
T4 (12 h)	−1692.7	198.4	310	131	2.01	4.53
T4 (18 h)	−1682.3	191.5	307	139	2.17	4.37

generation rate; thus, the as-cast alloys presented higher corrosion rate than the treated alloy. In addition, owing to the disappearance of the $Mg_{51}Zn_{21}$ secondary phases in the structure of the Mg–6Zn heat treated alloy, less galvanic couple occurred between $Mg_{51}Zn_{21}$ and α-Mg phases; therefore, Mg–6Zn treated specimen presented lower corrosion rate compared to the as-cast one. Corrosion rate of Mg–6Zn treated specimen decreased to 4.37 mm/year with increasing treatment time, owing to the role of the $Mg_{12}Zn_{13}$ secondary phases as micro-cathodes to increase the corrosion rate. Overall, the corrosion rate of treated Mg–6Zn is less than treated Mg–3Zn alloys. This can be attributed to the surface film covering Zn-containing magnesium alloys which suppresses the penetration of chloride anions into the magnesium hydroxide which provides a good barrier to improve the corrosion resistance. Also from the electrochemical parameters (i_{corr}, β_a and β_c) of specimens the polarisation resistance (R_P) was calculated according to the following equation [11]:

$$R_P = \frac{\beta_a \beta_c}{2.3(\beta_a + \beta_c) i_{corr}} \quad (2)$$

The polarisation resistance of the as-cast Mg–3Zn alloy and treated alloys showed relatively similar value in the range of 1.70–1.87 kΩ cm^2 which indicated less effect of treatment on the corrosion behaviour of the as-cast alloy which can be attributed to similar volume fraction of the precipitation phases in the crystal grains. However, T4 treatment enhanced the polarisation resistance of the as-cast Mg–6Zn alloy due to the decomposition of $Mg_{51}Zn_{21}$. The R_P value of T4 treated alloy for 6 h was 1.95 kΩ cm^2 which increased to 2.01 and 2.17 kΩ cm^2 for the samples heat treated 12 and 18 h, respectively. This indicated that secondary phases have a considerable effect on the corrosion behaviour of as-cast and treated alloys.

3.3 Immersion test

Figure 6 shows corrosion morphologies by SEM of as-cast Mg–3Zn, Mg–6Zn and heat treated alloys immersed in the Kokubo solution for 168 h. Figure 6a shows the formation of cracks and the formation of high amount of white precipitates on the crack layer of the Mg–3Zn alloy. The crack formation is owing to the dehydration of the corrosion product when drying in ambient atmosphere [4]. Heat treated Mg–3Zn also presented similar morphology to as-cast (Fig. 6b) owing to the existence of $Mg_{12}Zn_{13}$ secondary phase in the structure and formation of galvanic couples with the Mg matrix. The secondary phase has significant role playing as a micro-cathode to increase the corrosion rate. EDS analysis shows precipitates composed of high amounts of Mg and O, as well as a low amount of Ca and P (Point A). Increasing the Zn content to 6 wt% into binary Mg–Zn alloy leads to precipitation of higher amounts of bright particles on the crack layer as the entire film layer was covered with bright small particles (Fig. 6c). EDS analysis indicates that the bright particles are composed of O, Ca, P, Na, C and Mg which inferred hydroxyapatite (HA) formation on the alloy surface (Point B). However, heat treated alloy experienced fewer cracks indicating that the film layer is more compact, resulting in higher corrosion resistance (Fig. 6d). This is because the solution treatment reduces galvanic corrosion due to the decomposition of the $Mg_{51}Zn_{20}$ into α-Mg and $Mg_{12}Zn_{13}$, thus decreasing the corrosion rate of the alloy [12]. According to the corrosion mechanism, after exposing Mg based alloy to the SBF solution, at first magnesium alloys are dissolved and simultaneously a corrosion product begins to deposit on the sample surface [17]. The corrosion products formed are based on the following reactions:

$$Mg \rightarrow Mg^{+2} + 2e^- \quad (2)$$

$$2H_2O + 2e^- \rightarrow H_2 + 2OH^- \quad (3)$$

$$Mg^{2+} + 2OH^- \rightarrow Mg(OH)_2 \quad (4)$$

$$Mg(OH)_2 + Cl^- \rightarrow MgCl_2 + 2OH^- \quad (5)$$

According to reaction (2) (anodic reaction) and (3) (cathodic reaction), Mg transforms to stable Mg^{2+} ion; subsequently the cathodic reaction occurs accompanied by formation of hydroxide ion. The Mg^{2+} ion reacts with hydroxide ion and forms magnesium hydroxide [11]. By the evolution of $Mg(OH)_2$ as a barrier film, the degradation rate of the sample declines and corrosion products such as CO_3^{2-} and PO_4^{3-} ions precipitate on the surface of the specimen [4]. The presence of phosphates ion

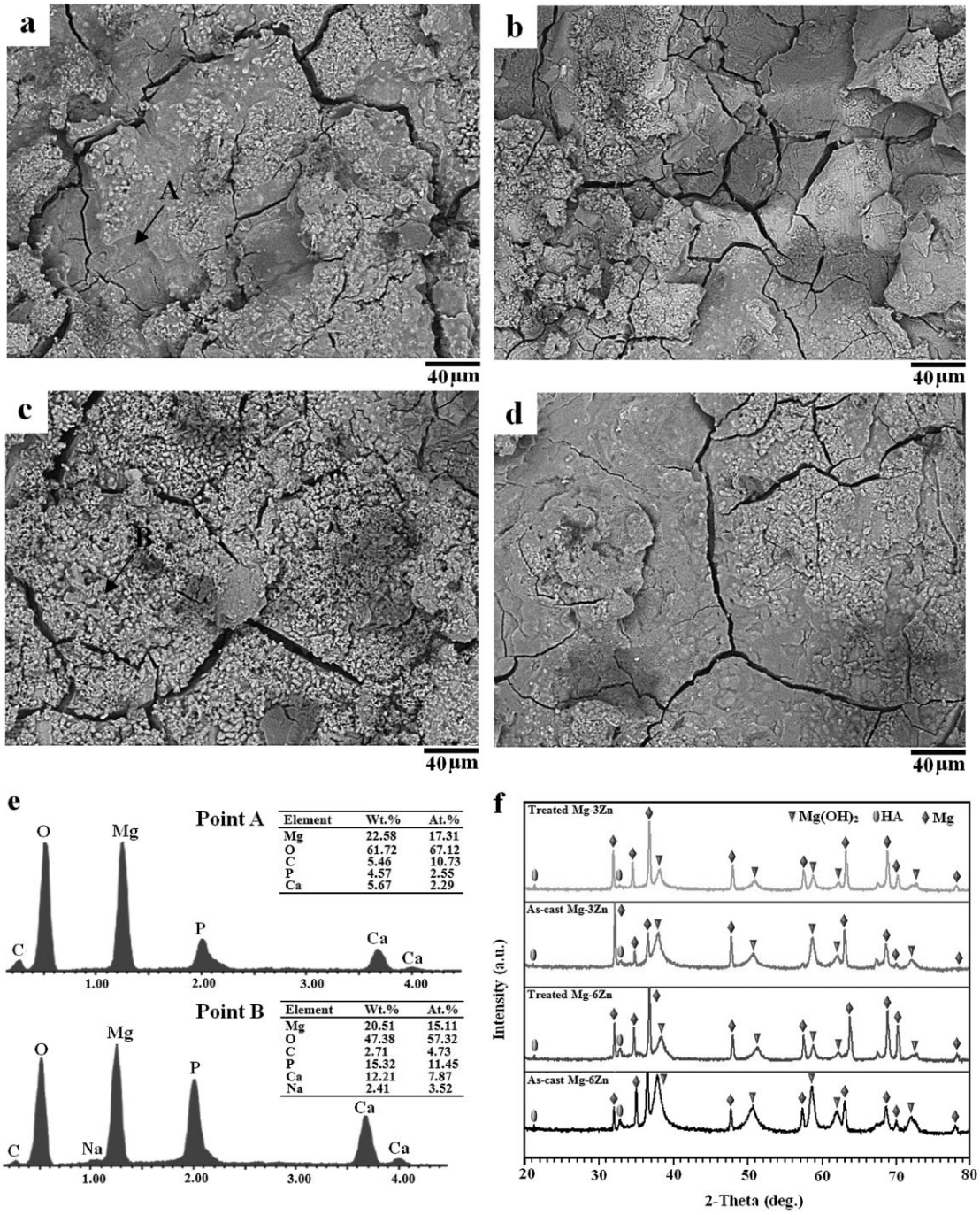

Figure 6. SEM micrographs of as-cast and T4 heat treated alloys after immersion into Kokubo for 168 h: (a) Mg–3Zn, (b) Mg–3Zn (6 h), (c) Mg–6Zn, (d) Mg–6Zn (6 h), (e) EDS analysis of points A and B in (a) and (c), and (f) X-ray diffraction patterns of the corrosion products of the as-cast and heat treated Mg–Zn alloys

(PO_4^{3-} or HPO_4^{2-}) in SBF can effectively slow down the dissolution of magnesium due to the formation of compact and insoluble phosphates. Corrosion products containing $Mg(OH)_2$ and HA also fill the corrosion pits and hence lead to more reduction of the degradation rate. Further increase in immersion time leads to the fact that barrier film became more dense, while the penetration of ions into the film was restricted causing the barrier film not to grow again. Regarding reaction (5), chloride ion reacts with the deposed $Mg(OH)_2$ on the specimens and forms $MgCl_2$ with higher solubility compared to $Mg(OH)_2$. There is a dynamic balance between dissolution and formation of barrier film on the surface of Mg, however due to chloride ion adsorbed on the surface film, the dynamic balance is not maintained. Therefore, chloride ion decreases the corrosion resistance of the specimens. Moreover, due to small radius of chloride ion, its easy penetration occurs in the corrosion film which causes the

preferential adsorption and replacement of the hydroxide ion by the chloride ion [11]. By progressing of the reaction, high amounts of Mg^{2+} are dissolved in the solution, thus more HCO_3^-, HPO_4^{2-} and Ca^{2+} react with OH^- to form HA which causes an increase in the corrosion resistance.

The XRD pattern of the as-cast and heat treated Mg–Zn specimens in the Kokubo solution after 168 h immersion proves the formation of $Mg(OH)_2$ accompanied by Mg and HA (Fig. 6f). The broader $Mg(OH)_2$ peaks were observed in the as-cast Mg–6Zn as the main corrosion products compared to the other alloys. In addition, $Mg(OH)_2$ peaks in both treated alloys are lower than the as-cast alloys indicating less corrosion attack in heat treated alloys. However, the presence of low amount of HA was observed in the corrosion products of the aforementioned alloy. At the earlier stage of the corrosion process, the $Mg(OH)_2$ forms which acts as a barrier film for the precipitation of calcium and phosphate. However, pits form due to chloride ions which resulted in the breakdown of the $Mg(OH)_2$. Thus, for the precipitation of hydroxyapatite on the Mg alloy surface, suppressing the evolution of $Mg(OH)_2$ film is vital. The pH variations of the SBF for the as-cast Mg–3Zn, Mg–6Zn and T4 heat treated alloys *versus* immersion time are shown in Fig. 7. This shows that the pH values of both as-cast Mg–Zn alloys increased from about 7.66 to 9.50 in the initial stage of immersion test. The T4 treated alloys encountered similar trends for various heat treatment times from 6 to 18 h. An early increase in pH values for specimen was caused by hydroxide ion accumulation as $Mg(OH)_2$ layer on the substrate [16]. Furthermore, the deposition of magnesium phosphate and carbonate accelerates due to the high pH value of the solution. However, this high pH value also resulted in local alkalisation which may negatively affect the pH value in the surrounding of the magnesium implant [6]. By increasing the immersion time to 168 h, the pH value of both as-cast Mg–Zn alloys gradually increased to around 9.70 representing a steady trend. This phenomenon is owing to the evolution of $Mg(OH)_2$ film and the precipitation of calcium phosphate as a top layer on the $Mg(OH)_2$ which acts as an inner layer [17]. At the same time, due to consuming the calcium phosphate from the solution, the amount of hydroxyapatite precipitation on the surface increased. A similar trend is also observed for T4 heat treated alloys where the pH values steadily increased to the 9.50–9.80 range.

The average mass loss of the as-cast Mg–3Zn, Mg–6Zn and T4 heat treated alloys *versus* immersion time in Kokubo solution for 168 h are indicated in Fig. 8. The average corrosion rate of T4 heat treated Mg–3Zn for various treatment times of 6, 12 and 18 h were 1.92, 1.87 and 1.85 mm/year, respectively. These values are very close to the corrosion rate of as-cast Mg–3Zn (1.95 mm/year). However, after heat treatment of as-cast Mg–6Zn for 6 h, the corrosion rate decreased from 3.48 to 1.42 mm/year. This is owing to the dissolution of the $Mg_{51}Zn_{20}$ secondary phase into the α-Mg matrix and $Mg_{12}Zn_{13}$ reducing galvanic corrosion. Besides, increasing the heat treatment time to 12 and 18 h leads to a slight decrease in corrosion rate to 1.38 and 1.36 mm/year, respectively. This is because a high amount of secondary phase was decomposed in the first 6 h of heat treatment; hence, the amount

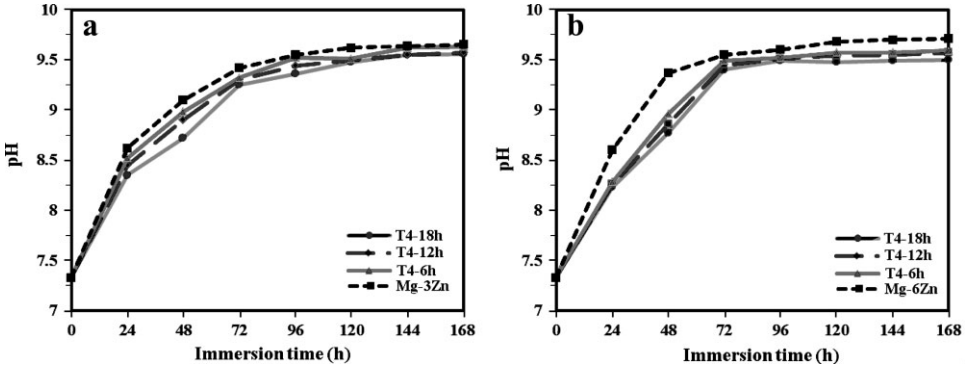

Figure 7. The variation of the pH value in Kokubo solution as a function of immersion time for (a) Mg–3Zn and (b) Mg–6Zn alloys heat treated for different times

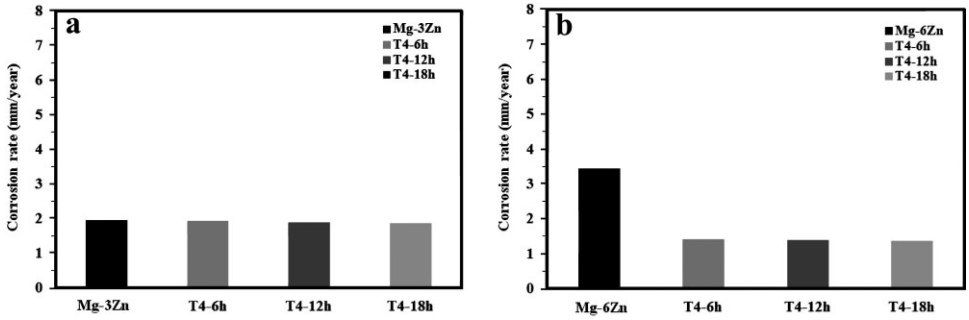

Figure 8. Corrosion rate obtained by weight loss of (a) Mg–3Zn and (b) Mg–6Zn before and after heat treatment for different durations and after immersion in Kokubo solution for 168 h

of galvanic corrosion remained unchanged after treatment beyond 6 h.

4 Conclusions

As-cast Mg–3Zn alloy reveals the presence of α-Mg and $Mg_{12}Zn_{13}$ phases while as-cast Mg–6Zn alloy shows the presence of α-Mg, $Mg_{12}Zn_{13}$ and $Mg_{51}Zn_{20}$ phases. After T4 treatment of the Mg–6Zn alloy, the amount of secondary phases changed, while, Mg–3Zn shows the same amount of secondary phases. The T4 heat treated Mg–6Zn alloy showed the lowest corrosion rate in simulated body fluid due to the decomposition of $Mg_{51}Zn_{20}$. However, T4 treated Mg–3Zn alloy with a large number of precipitates ($Mg_{12}Zn_{13}$) showed the highest corrosion rate. This is due to galvanic couple formation between Mg matrix and the secondary phases. Increasing heat treatment time from 6 to 18 h, has a less significant influence on the degradation rate of both alloys which is owing to the unchanged microstructure after heat treatment beyond 6 h.

5 References

[1] J. G. Li, Y. Lv, H. W. Wang, *Mater. Corros.* **2013**, *64*, 426.
[2] G. Ben-Hamu, D. Eliezer, *Mater. Corros.* **2013**, *64*, 516.
[3] L. Wang, T. Zhou, J. Liang, *Mater. Corros.* **2012**, *63*, 713.
[4] L. Yang, N. Hort, D. Laipple, D. Höche, *Acta Biomater.* **2013**, *9*, 8475.
[5] P. Rosemann, J. Schmidt, A. Heyn, *Mater. Corros.* **2013**, *64*, 714.
[6] G. Song, *Corros. Sci.* **2007**, *49*, 1696.
[7] F. Witte, N. Hort, C. Vogt, S. Cohen, K. U. Kainer, R. Willumeit, F. Feyerabend, *Curr. Opin. Solid State Mater. Sci.* **2008**, *12*, 63.
[8] X. Zhang, G. Yuan, L. Mao, *J. Mech. Behav. Biomed.* **2012**, *7*, 77.
[9] Y. Song, E. Han, D. Shan, C. D. Yim, B. S. You, *Corros. Sci.* **2012**, *60*, 238.
[10] P. Hoyer, G. L. Angrisani, C. Klose, *Mater. Corros.* **2012**, *63*, 1.
[11] H. R. Bakhsheshi-Rad, M. H. Idris, M. R. Abdul-Kadir, *Surf. Coat. Tech.* **2013**, *222*, 79.
[12] W. Zhou, T. Shen, N. N. Aung, *Corros. Sci.* **2010**, *52*, 1035.
[13] X. Zhang, K. Zhang, X. Li, et al., *J. Rare Earth* **2012**, *30*, 1158.
[14] T. Kokubo, H. Takadama, *Biomaterials* **2006**, *27*, 2907.
[15] P. Ghosh, M. Mezbahul-Islam, M. Medraj, *CALPHAD* **2012**, *36*, 28.
[16] H. R. Bakhsheshi-Rad, M. H. Idris, M. R. A. Kadir, M. Daroonparvar, *Trans. Nonferrous Met. Soc. China* **2013**, *23*, 699.
[17] Y. Song, S. Zhang, J. Li, C. Zhao, X. Zhang, *Acta Biomater.* **2010**, *6*, 1736.

(Received: November 3, 2013) W7492
(Accepted: November 24, 2013)

